PAPER

Semimetal to semiconductor transition and polymer electrolyte gate modulation in single-crystalline bismuth nanowires

Jeongmin Kim and Wooyoung Lee*

A semimetal to semiconductor transition in low-dimensional Bi nanowires is theoretically predicted based on the quantum confinement effect, which results in the enhancement of the thermoelectric performance. However, this transition has rarely been observed in the transport properties of gate modulation because of there being too few charge carriers induced by a typical electric field effect. In this paper, we report on our observations of the on–off state in a Bi nanowire using a polyethylene oxide/$LiClO_4$ electrolyte gate, which produces a much larger effect than a back-gate. The carrier density of the surface state was found to be consistent with previously reported results. The intrinsic properties of the Bi nanowires, as obtained by temperature- and diameter-dependent gate modulations, are also discussed.

Introduction

The semimetal to semiconductor (SMSC) transition due to the quantum confinement effect in low-dimensional bismuth (Bi) has been intensively investigated since it was first predicted by theoretical calculations.[1,2] This transition phenomenon originates from the unique properties of semimetal Bi including the small band-overlap energy (3 meV), small effective mass (0.001 m_e), and long Fermi wavelength (70 nm).[3–5] In particular, Bi nanowires (NWs) have been widely employed for low-dimensional thermoelectrics because their thermoelectric performance can be enhanced by the SMSC transition.[6] However, despite the development of various growth methods for low-dimensional Bi NWs, the experimental demonstration of this transition based on electrical transport has rarely been reported.[7–9] In practice, it is difficult to verify that the band gap opening from the magneto-transport properties and the transition cannot be determined solely from the semiconducting temperature coefficient of the resistance of a Bi NW.[10–13] Moreover, the expected enhancement of the Seebeck coefficient has not been confirmed at the predicted critical diameter at which the SMSC transition occurs.[8,14–16] Although a significantly enhanced Seebeck coefficient was demonstrated using the quantum point contact of Bi obtained by the electromigration effect, the dimension of Bi was found to be much smaller than the predicted diameter.[17] This inconsistency can be attributed to the strong electron–hole coupling effect between the conduction and valence sub-bands at the L-point of Bi.[5] As the diameter decreases, the increase in the effective electron mass caused by the coupling effect causes the critical diameter to decrease according to the relationship between the quantum confinement effect and the carrier effective mass.[18] Furthermore, the carriers induced from the surface states of the Bi dominate the bulk carriers at diameters of less than 50 nm, resulting in two-dimensional transport characteristics.[13,15,19] Because of the high density of the Bi surface carriers, it is challenging to verify the band gap opening by the field effect gate modulation using a typical back-gate structure such as the Si/SiO_2 substrate. However, a polymer electrolyte gate can be used to deal with such a large amount of charge carriers. Particularly, polyethylene oxide (PEO)/$LiClO_4$ has been used to demonstrate the strong gate effect and low gate voltage operation of nano-materials.[20–22]

In this work, we studied the gate-modulated transport properties of single-crystalline Bi NWs with diameters between 18 and 250 nm to investigate the change in the intrinsic properties and SMSC transition in terms of the diameter (d). The back-gate effect when using a Si/SiO_2 substrate and the polymer electrolyte gate effect when using PEO/$LiClO_4$ were used to generate a sufficiently large electric field corresponding to the high surface carrier density of Bi.[20,23] The electric field effect produced by the electrolyte gate was found to be several orders of magnitude larger than that of the back-gate. The reversible on/off switching and the obtained carrier density are consistent with the predicted SMSC transition and the reported surface carrier density of Bi, respectively.

Department of Materials Science and Engineering Yonsei University, 50 Yonsei-ro, Seodaemun-gu 03722, Korea. E-mail: wooyoung@yonsei.ac.kr

Experimental section

Single-crystalline Bi NWs were obtained by the spontaneous growth of Bi NWs on the Bi film, termed the "on-film formation of nanowire" (OFFON).[9] High-quality Bi NWs were grown by releasing the thermal stress during the annealing process (250 °C for 5 h) of the 50 nm Bi film deposited by using a specially made ultrahigh vacuum (UHV) sputtering system. Bi NWs having a range of diameters were obtained using the grain size control of the Bi films.[12] High-resolution transmission electron microscopy analysis revealed that the crystalline structure of the NWs was aligned with the [100] orientation of the Bi (binary axis).[16] We successfully fabricated Bi NW devices with diameters of 18, 40, 60, 90, 150, and 250 nm and four-point contact, using a typical electron-beam lithography system (JSM-7001F JEOL and ELPHY Quantum Raith). To obtain ohmic contact, the Bi oxide layer on the surface of the NWs was removed by using a specially made Ar plasma etching system, after which Cr/Au electrodes (5 nm/200 nm) were deposited using the UHV sputtering system. The details of the sample preparation are available in the literature.[13,16,18] The transport properties were measured by using a DAQ module (6251BNC NATIONAL INSTRUMENTS) and a nanovoltmeter (2182A KEITHLEY) using the four-probe method to remove the contact resistance between each Bi NW and the electrodes. A voltage divider was applied to the current source to provide overpower protection at the high resistance off-state, while a source-meter system (2400 KEITHLEY) was used to generate the gate voltage (V_G). In the measurement of gate modulations, the current–voltage sweeps were independently performed at each gate voltage point instead of increasing the number of points, in order to reduce damage to electrically vulnerable Bi NWs and to obtain convincing data.

Results and discussion

Electric field gate modulations

Fig. 1 shows the schematic images of the field effect gate modulation measurements using the back-gate and the polymer electrolyte gate. Conventionally, gate modulation is done using the back-gate and a highly doped Si/SiO$_2$ substrate, because additional processes for the dielectric layer and the gate electrodes are not necessary (Fig. 1(a) and (c)). However, the charge density as doped by the electric field effect of the back-gate based on the Si/SiO$_2$ substrate is insufficient to investigate the SMSC transition. The doped charge density of the back-gate using the Si/SiO$_2$ substrate is defined as

$$n_d = \left(\frac{C}{et_{SiO_2}d_{Bi}}\right)V_G \quad (1)$$

where C, t_{SiO_2}, and d_{Bi} are the capacitance, thickness of the SiO$_2$ layer (500 nm), and diameter of the Bi NW,
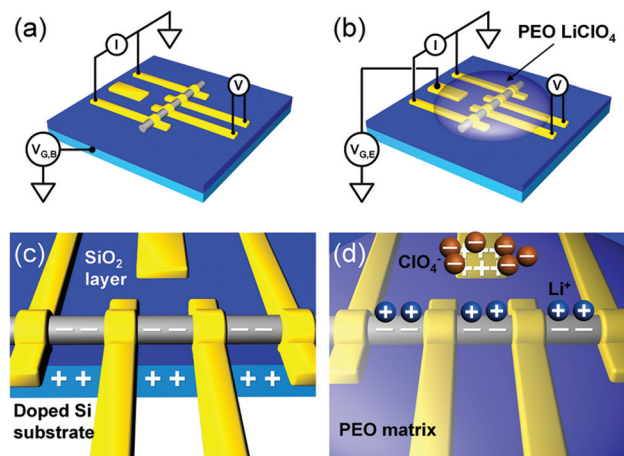
Fig. 1 Gate modulation measurements and electric field effect mechanism. (a), (c) For back-gate using a highly doped Si/SiO$_2$ substrate and (b), (d) for a polymer electrolyte gate using PEO/LiClO$_4$. Here I, V, $V_{G,B}$, and $V_{G,E}$ are the source current, measured voltage drop, back-gate voltage, and electrolyte gate voltage, respectively.

respectively.[9,24] The capacitance of the back-gate (C_B) is defined as

$$C_B = \frac{2\pi(\varepsilon_0\varepsilon_{SiO_2})}{\ln\left(\frac{2t_{SiO_2}}{r_{Bi}}\right)} \quad (2)$$

using the cylinder-above-plane model, where ε_0, ε_{SiO_2}, and r_{Bi} are the permittivity of free space, permittivity of SiO$_2$, and radius of the Bi NW, respectively.[20] As the diameter decreases from 250 to 18 nm, although the calculated n_d at a gate voltage of 40 V increases from 2.05×10^{17} to 1.26×10^{18} cm^{-3}, the values are smaller than the bulk carrier density of Bi at room temperature (3×10^{18} cm^{-3}).[25] Even at the 100-V-gate voltage, which is much larger than the break down voltage of the Bi/SiO$_2$/Si structure, n_d is not enough to deplete the carriers induced from the surface states of the Bi. Moreover, the effective charge density can be reduced by the screening effect, when the NW is thicker than the screening length (40 nm in Bi).[24]

In this system, the doped charge density is limited by the thickness and capacitance of the dielectric material.[21] Furthermore, the dielectric materials can break down at very high gate voltages, which are required to obtain a significantly high doping state. Although high-κ dielectric materials can be employed to enhance the gate effect, the additional processes needed to form the dielectric materials present a challenge when working with low melting point materials such as Bi, and are still prone to the breakdown issue. Polymer electrolyte gate modulation was considered as a means of demonstrating the high doping state.[20] When using this method, the ions form a double layer on the NW and electrodes, which induce counter charges according to the gate voltage, as shown in Fig. 1(b) and (d). The electrolyte gate effect is realized by a significantly lower gate voltage without an electrochemical

reaction, relative to that of a typical back-gate, because the mobile ions in the polymer matrix can produce a nanometer-size gate.[21,23] The capacitance of the electrolyte gate (C_E) is given by[20]

$$C_E = \frac{2\pi(\varepsilon_0 \varepsilon_{polymer})}{\ln\left(\frac{r_{Bi} + \lambda_D}{r_{Bi}}\right)} \tag{3}$$

where $\varepsilon_{polymer}$ and λ_D are the permittivity of the polymer matrix and the Debye screening length, respectively.[20] The values of C_E of our systems can be calculated by assigning $\varepsilon_{polymer} = 5$ and $\lambda_D = 1$ nm.[20,21] The calculated C_E (2.64×10^{-9} F m^{-1}) is more than 50 times that of the calculated C_B (4.54×10^{-11} F m^{-1}) for the 18 nm-diameter. The large-magnitude charge density, doped by the polymer electrolyte gate with significantly high capacitance, can deplete the carriers induced by the surface and bulk energy states of Bi. The polymer electrolyte consisting of PEO and LiClO$_4$ was dispersed using a drop-casting method on the single Bi NW device, followed by a baking process.

Temperature dependence

Fig. 2 shows the temperature-dependent transport properties. Although the large Bi NW with a diameter of 150 nm exhibits a metallic temperature dependency of conductivity (σ) similar to bulk Bi, the small Bi NWs (d = 18 and 40 nm) mainly exhibit nonmonotonic behavior (Fig. 2(a)).[16,25] Because the semimetallic Bi has a very small carrier density ($n = 3 \times 10^{17} - 3 \times 10^{18}$ cm^{-3} at 2–300 K) relative to a typical metal, and the spatial confinement of the NW reduces the temperature dependency of the carrier mobility (μ), the conductivity can be affected by the carrier density as well as the mobility depending on the temperature.[13,18,25] The inset indicates that the conductivity was determined predominantly by the carrier mobility at temperatures less than about 100 K. This phenomenon is consistent with the temperature dependency of the gate-modulated conductivity (Fig. 2(b)). The slope of the gated conductivity (conductance, G) is related to the carrier mobility defined by the following relationship[9]

$$\frac{dG}{dV_G} \propto \frac{d\sigma}{dV_G} \propto \mu. \tag{4}$$

Therefore, the increase in the slope as the temperature decreases indicates higher mobility at lower temperatures. The inset shows the slope values at each temperature. Consequently, a decrease in the temperature leads not only to an increase in the carrier mobility but also enhances the contribution of the mobility to the conductivity.

Diameter dependence

Fig. 3 shows the diameter-dependent back-gate-modulated transport properties of Bi NWs, presented as a function of gate voltage at room temperature. The positive slope of the gated conductivity indicates that the major carriers of the Bi NWs are electrons. The measured conductivities at a zero gate voltage and the slopes of the gated conductivities of Bi NWs
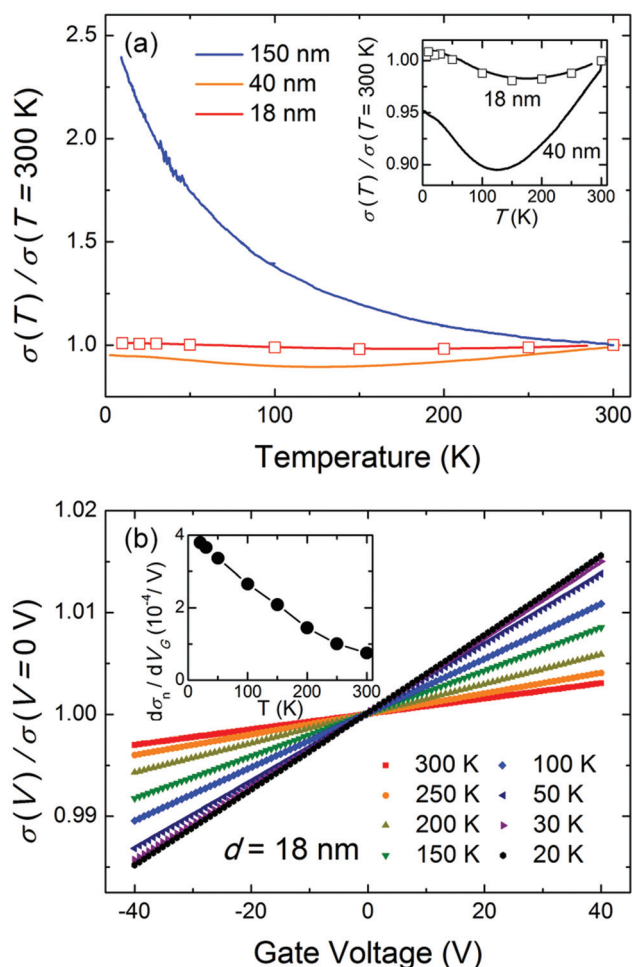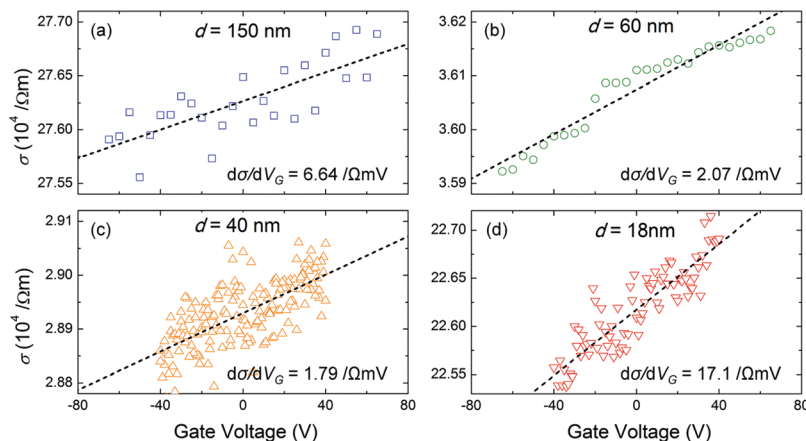

Fig. 2 Temperature-dependent transport properties. (a) Temperature-dependent conductivities of Bi NWs with diameters of 18, 40, and 150 nm. The conductivity is normalized with that of room temperature. The solid line and open squares indicate the measurements taken during continuous temperature ramping and after temperature stabilization, respectively. The inset shows the temperature-dependent behavior of the 18- and 40 nm NWs in detail. (b) Back-gate-modulated conductivity of 18 nm Bi NW at various temperatures. The conductivity is normalized with that of the zero gate voltage. The inset shows the slope of the normalized gate-modulated conductivity as a function of temperature.

with diameters of 150, 60, 40, and 18 nm are 2.76 ($\pm$0.16) $\times 10^5$, 3.60 ($\pm$0.20) $\times 10^4$, 2.89 ($\pm$0.17) $\times 10^4$, and 2.26 ($\pm$0.13) $\times 10^5$ Ω^{-1} m^{-1}, and 6.64 ($\pm$1.11), 2.07 ($\pm$0.11), 1.79 ($\pm$0.15), and 17.1 ($\pm$0.96) Ω^{-1} m^{-1} V^{-1}, respectively. For diameters in the range of 40–150 nm, a decrease in the diameter leads not only to a decrease in the conductivity but also reduces the mobility according to eqn (4). The estimated carrier mobilities are given in the next section as a table. This can be attributed to a decrease in the mean free path originating from the carrier nonspecular surface scattering due to the spatial confinement and the increase in the carrier effective mass owing to the strong coupling effect caused by sub-band shifting.[13,18] Whereas, in the smallest NW (18 nm), the conductivity is comparable to that of the 150 nm Bi NW, which is much larger

Fig. 3 Diameter-dependent transport properties. Conductivity of Bi NWs with diameters of (a) 150, (b) 60, (c) 40, and (d) 18 nm as a function of the back-gate voltage at room temperature. The slope of the gated conductivity decreases with the diameter for diameters in the range of 150−40 nm.

than that for Bi NWs with diameters of 40 and 60 nm. Moreover, the slope value exhibits the largest mobility. This change in the transport properties is probably due to the metallic surface states of Bi, as reported in previous studies.[16,19,26] For values of less than 50 nm in Bi, the surface state effect dominates the bulk transport properties because of the large surface to volume ratio.[19] Particularly, in the Bi NWs grown along the binary axis, the transition arises at diameters less than 40 nm.[16] In this gate modulation using the back-gate, however, we could not obtain precise values for the carrier mobility and density. In typical semiconductors with a single major electronic energy band, the intrinsic properties can be calculated based on the relationship, $d\sigma/dV_G = e\mu$ (dn_d/dV_G). In semimetal Bi, however, a two-band model should be employed to investigate the conductivity because there are two major bands for the electrons and holes resulting in the total conductivity, $\sigma_{total} = \sigma_e + \sigma_h = en\mu_e + ep\mu_h$. For this reason, the changes in the slope at the band edge for the gate-modulated conductivity should be used to estimate the intrinsic properties of Bi.[9,24] With back-gate modulation, however, the doped charge density is not sufficient to vary the Fermi energy level to the band edge even at a gate voltage of ±65 V. Furthermore, the carrier density induced from the surface states, which should be depleted to observe the band gap opening, is significantly high relative to the back-gate effect. Therefore, a more powerful electric field effect is needed to investigate the SMSC transition in low-dimensional Bi.

Electrolyte gate modulations

Fig. 4 shows the gate-modulated transport properties of Bi NWs using a polymer electrolyte gate, presented as a function of gate voltage at room temperature. Note that the dispersed polymer electrolyte decreases the conductivity, even at a zero gate voltage. The gate voltage, at which the initial conductivity before polymer electrolyte dispersion is obtained, is presented as a colored solid line in Fig. 4(a), (b), and (d) inset. The initial states of the 250- and 150 nm-diameter NWs exhibit positive

slopes, indicating that the transport properties are dominated by the electrons. The slopes vary as the gate voltage is decreased, with even the 150 nm NW exhibiting a negative slope below a gate voltage of approximately −2 V. Although the gate voltages leading to these changes in the slope have not been clarified, the carrier density can be estimated from eqn (1) and (3).[9,24] In the 250- and 150 nm NW, the carrier densities were found to be larger than 3.49×10^{18} cm^{-3} and approximately 3.61×10^{18} cm^{-3}, which were calculated using 6 V (1 V to −5 V) and 5 V (2 V to −3 V) gate modulations, respectively. These estimated values are consistent with the bulk carrier density of Bi at room temperature (3×10^{18} cm^{-3}).[25] Using the estimated carrier densities and measured conductivities, the carrier mobilities of Bi NWs with diameters of 250 and 150 nm were calculated to be 4296 (±233) and 4780 (±277) cm^2 V^{-1} s^{-1}, respectively, which are four times smaller than that of the 400 nm Bi NW reported in a previous study, indicating a decrease in the mean free path of the electrons due to the carrier nonspecular surface scattering.[27] In the case of the 90 nm NW, although a negative slope was observed below a gate voltage of −5 V, the initial conductivity state (4.44 (±0.23) $\times 10^5$ Ω^{-1} m^{-1}) seems to fall outside the measured gate voltage range (Fig. 4(c)). As a result, the carrier density of this NW could not be obtained.

The electrolyte gate modulation in a Bi NW with a diameter of 18 nm exhibits a significantly large variation in the conductivity compared to those of the other NWs (Fig. 4(d)). The conductivity exhibits a reversible on–off recovery with negative gate voltages indicating the formation of a band gap caused by the SMSC transition. Note that the changes in conductivity, which are caused by any trouble in measurement such as electric damage on the NW and dielectric breakdown, were irreversible in our measurement. Although a hysteresis was observed in the on–off recovery, which can be attributed to the instability of the mobile ions in the polymer matrix, it can be minimized by reducing the voltage sweep rate.[23] The conductivity values at an electrolyte gate voltage of about 8 V is
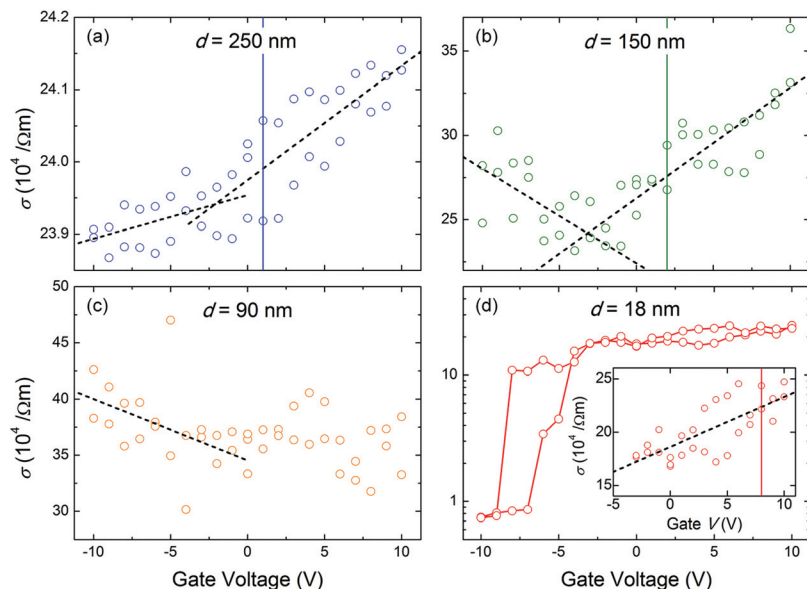
Fig. 4 Polymer electrolyte gate-modulated conductivities. Conductivity of Bi NWs with diameters of (a) 250, (b) 150, (c) 90, and (d) 18 nm as a function of the gate voltage at room temperature. The inset of (d) shows the electrolyte-gated conductivity for a range of gate voltages from −5 to 10 V.

similar to that at a zero back-gate voltage. Therefore, it can be considered that more than 13 V is needed to attain the off-state. The carrier density of the 18 nm Bi NW is estimated to be $n = 1.83 \times 10^{19}$ cm^{-3}, according to eqn (1) and (3). This three-dimensional bulk density is converted to a two-dimensional surface density, $n_s = 8.0 \times 10^{12}$ cm^{-2} by a relationship $n = 2n_s/r$, which is comparable to the reported surface state density for Bi (5.0×10^{12} cm^{-2}).[13,19] The obtained transport properties for the NWs studied are given in Table 1.

Fig. 5 displays the SMSC transition in the Bi NW with a diameter of 18 nm by the current–voltage (I–V) characteristics and temperature-dependent resistance with a variation of the gate voltage. To obtain the changes in the NW without the contact resistance, the four-probe configuration was used. The I–V curve is linear at positive gate voltages and the resistance is determined to be 7.09×10^4 Ω in the initial state (8 V) (Fig. 5(a)). This linear I–V curve is maintained for gate voltages in the range of −4–10 V, even though the variation of resistances with the gate voltages is slightly noisy, as indicated in Fig. 4(d). Interestingly, the I–V curve changes to non-linear with an increase of resistance at a gate voltage of −5 V. As illustrated in the inset of Fig. 5(a), the I–V curve becomes further
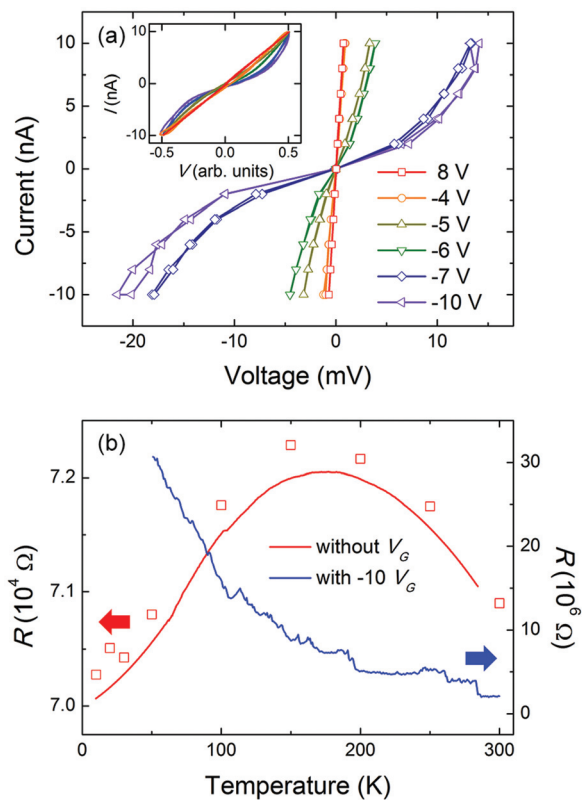
Fig. 5 SMSC transition in the Bi NW with a diameter of 18 nm. (a) I–V characteristics with a variation of the polymer electrolyte gate voltage. The inset indicates the change of linearity in the I–V curve with the gate voltages by normalization. (b) Temperature-dependent resistance with and without the electrolyte gate effect. The line data were collected by a voltage divider to protect the NW from overvoltage in continuous variation of temperature. The red squares were obtained at stabilized temperatures without the voltage divider.

Table 1 Electrical conductivity, carrier density, and mobility of Bi NWs

d (nm)	σ (10^4 Ω^{-1} m^{-1})	n (10^{18} cm^{-3})	μ (cm^2 V^{-1} s^{-1})
250	24.0 ± 1.3	3.49	4296 ± 233
150	27.6 ± 1.6	3.61	4780 ± 277
90	44.4 ± 2.3	—	—
60	3.60 ± 0.20	1.51 ± 0.08	1490
40	2.89 ± 0.17	1.40 ± 0.08	1289
18	22.6 ± 1.3	18.3	772 ± 44

nonlinear as the gate voltage decreases below −5 V and the resistance increases to two-order higher than that of the initial state at −10 V (2.09×10^6 Ω). Furthermore, the change in the temperature-dependent resistance also indicates the SMSC transition (Fig. 5(b)). As described in Fig. 2(a), the resistance of 18 nm-NW exhibits non-monotonic behavior with temperature. Without the gate effect, although the resistance increases with temperature above approximately 200 K because of the suppression of the mobility-dependency due to the surface scattering, the metallic behavior dominates the resistance in the low-temperature range (<200 K). Conversely, the temperature-dependent resistance becomes semiconducting with a gate voltage of −10 V, wherein the resistance monotonically increases with the decreasing temperature in the measured temperature range.

In the previous studies of Bi NWs grown by the OFF–ON technique, it was reported that the carriers induced from the surface states are predominantly responsible for the transport properties at diameters of less than 40 nm.[13,16] The metallic surface carriers increase the conductivity to a level similar to that of bulk Bi and have two-dimensional characteristics.[13,16] The Bi NW surface states could also be found from Bi NWs grown by different methods.[6,11,15,26] The electrolyte gate modulation of the smallest Bi NW is in good agreement with the results of previous studies and the formation of a band gap as predicted by the SMSC transition. Although the first predicted critical diameter occurring at the SMSC transition is smaller than 50 nm, the band gap opening is observed at a diameter of 18 nm with a significantly large electric field effect because of the strong coupling effect in the L-point sub-bands and the metallic surface states, which leads to a decrease in the critical diameter and hides the band gap, respectively.[16]

Conclusions

In summary, the gate-modulated transport properties of single-crystalline Bi NWs grown by the OFF–ON method were measured by using the Si/SiO_2 back-gate and the $PEO/LiClO_4$ polymer electrolyte gate effects. The temperature-dependent conductivity and the back-gate effect indicate that the carrier mobility is predominant in transport at low temperatures. The diameter dependency of the gated conductivity confirmed that the mobility decreases with the diameter because of the spatial confinement and the strong coupling effect, which originate from the classical size and quantum confinement effects, respectively. Depletion of the carriers in Bi NWs was attained by the polymer electrolyte gate effect, which is more than 50 times greater than the back-gate effect based on the SiO_2/Si substrate. The surface carrier density was found to be 8.0×10^{12} cm^{-2}. Our investigation results indicated reversible on–off states in a low-dimensional Bi NW, which is consistent with the SMSC transition expected in the theoretical studies.

Acknowledgements

Notes and references

1 M. S. Dresselhaus, G. Dresselhaus, X. Sun, Z. Zhang, S. B. Cronin and T. Koga, *Phys. Solid State*, 1999, **41**, 679–682.

2 Y. M. Lin, X. Z. Sun and M. S. Dresselhaus, *Phys. Rev. B: Condens. Matter Mater. Phys.*, 2000, **62**, 4610–4623.

3 Z. B. Zhang, X. Z. Sun, M. S. Dresselhaus, J. Y. Ying and J. Heremans, *Phys. Rev. B: Condens. Matter Mater. Phys.*, 2000, **61**, 4850–4861.

4 S. B. Cronin, Ph.D. Thesis, Massachusetts Institute of Technology, 2002.

5 T. W. Cornelius and M. E. T. Molares, *Nanowires*, InTech, Shanghai, 2010.

6 J. Kim, W. Shim and W. Lee, *J. Mater. Chem. C*, 2015, **3**, 11999–12013.

7 Z. Zhang, J. Y. Ying and M. S. Dresselhaus, *J. Mater. Res.*, 1998, **13**, 1745–1748.

8 A. Nikolaeva, T. E. Huber, D. Gitsu and L. Konopko, *Phys. Rev. B: Condens. Matter Mater. Phys.*, 2008, **77**, 035422.

9 W. Shim, J. Ham, K. I. Lee, W. Y. Jeung, M. Johnson and W. Lee, *Nano Lett.*, 2009, **9**, 18–22.

10 J. Heremans, C. M. Thrush, Z. Zhang, X. Sun, M. S. Dresselhaus, J. Y. Ying and D. T. Morelli, *Phys. Rev. B: Condens. Matter Mater. Phys.*, 1998, **58**, R10091–R10095.

11 A. Nikolaeva, D. Gitsu, L. Konopko, M. J. Graf and T. E. Huber, *Phys. Rev. B: Condens. Matter Mater. Phys.*, 2008, **77**, 075332.

12 S. Lee, J. Ham, K. Jeon, J.-S. Noh and W. Lee, *Nanotechnology*, 2010, **21**, 405701.

13 J. Kim, S. Lee, Y. M. Brovman, M. Kim, P. Kim and W. Lee, *Appl. Phys. Lett.*, 2014, **104**, 043105.

14 J. Heremans and C. M. Thrush, *Phys. Rev. B: Condens. Matter Mater. Phys.*, 1999, **59**, 12579–12583.

15 T. E. Huber, A. Adeyeye, A. Nikolaeva, L. Konopko, R. C. Johnson and M. J. Graf, *Phys. Rev. B: Condens. Matter Mater. Phys.*, 2011, **83**, 235414.

16 J. Kim, S. Lee, Y. M. Brovman, P. Kim and W. Lee, *Nanoscale*, 2015, **7**, 5053–5059.

17 E. Shapira, A. Holtzman, D. Marchak and Y. Selzer, *Nano Lett.*, 2012, **12**, 808–812.

18 J. Kim, D. Kim, T. Chang and W. Lee, *Appl. Phys. Lett.*, 2014, **105**, 123107.

19 P. Hofmann, *Prog. Surf. Sci.*, 2006, **81**, 191–245.

20 C. Lu, Q. Fu, S. Huang and J. Liu, *Nano Lett.*, 2004, **4**, 623–627.

21 A. Pachoud, M. Jaiswal, P. K. Ang, K. P. Loh and B. Özyilmaz, *Europhys. Lett.*, 2010, **92**, 27001.

22 D. Liang and X. P. A. Gao, *Nano Lett.*, 2012, **12**, 3263–3267.

23 M. J. Panzer, C. R. Newman and C. D. Frisbie, *Appl. Phys. Lett.*, 2005, **86**, 103503.

24 A. Boukai, K. Xu and J. R. Heath, *Adv. Mater.*, 2006, **18**, 864–869.

25 J. Heremans, C. M. Thrush, Y. M. Lin, S. Cronin, Z. Zhang, M. S. Dresselhaus and J. F. Mansfield, *Phys. Rev. B: Condens. Matter Mater. Phys.*, 2000, **61**, 2921–2930.

26 T. E. Huber, A. Nikolaeva, L. Konopko and M. J. Graf, *Phys. Rev. B: Condens. Matter Mater. Phys.*, 2009, **79**, 201304(R).

27 K. Lee, S. Lee, S. N. Holmes, J. Ham, W. Lee and C. H. W. Barnes, *Phys. Rev. B: Condens. Matter Mater. Phys.*, 2010, **82**, 245310.